

JOINT INSTITUTE FOR NUCLEAR RESEARCH
VEKSLER AND BALDIN LABORATORY OF HIGH ENERGY
PHYSICS

**FINAL REPORT ON THE STUDENT PROGRAM at
JINR 2022**

Particle identification in heavy ion collisions in MPD at NICA

Supervisor:

Dr. Alexey Aparin

Student:

Pedro Antonio Nieto Marín,
Universidad Autónoma de Sinaloa

Dubna, 2022

Abstract

To make an analysis of identified charged particles (π^\pm , K^\pm and p^\pm) formation at midrapidity region of $|\eta| < 0.5$ we calculated centrality classes for Bi+Bi collisions at center-of-mass energies of $\sqrt{S_{NN}} = 7.7, 9, 9.2$ GeV generated by the statistical Monte Carlo generator model: Ultrarelativistic Quantum Molecular Dynamics (UrQMD). We obtained the multiplicity distributions from the data reconstructed by the TPC in the MpdRoot framework to calculate the centrality classes. To do the Particle Identification (PID) we used the z-variable method for narrow ranges of transverse momentum p_T in the energy loss $\langle dE/dx \rangle$ vs p_T for protons, pions and Kaons. Finally, we implemented the Bethe-Bloch formula fit for five parameters to identify each particle and we reported it.

Introduction

The Quark-Gluon Plasma (QGP) has been studied to understand the first instants of the universe (about a microsecond after the Big Bang) and its properties. Large experimental facilities such as LHC and RHIC are looking for physical observables to help us find the phase transition from hadronic matter to the QGP at which the deconfinement of quarks and gluons occurs in the quantum chromodynamics (QCD) phase diagram. The main goal is to form and characterize a state of unconfined quarks and gluons in local thermal equilibrium in the heavy ion collisions to investigate the properties of the hadronic matter and recreate the QGP.

Figure 1 shows a conjecture of the QCD phase diagram showing the transitions between the phases of hadronic matter and QGP. The relationship between chemical potential (μ_B) and temperature (T) are the main parameters to understand the properties of these created matter [1]. Lattice QCD has been of great relevance as the main tool for the theoretical study of phase transitions predictions for more than 40 years, but only at a chemical potential close to zero it has been very successful in predicting observables in very high energy experiments

at LHC or RHIC. However, it presents a very big problem in obtaining predictions for a chemical potential greater than zero, which is fundamental if we want to investigate the phase transitions and the critical point.

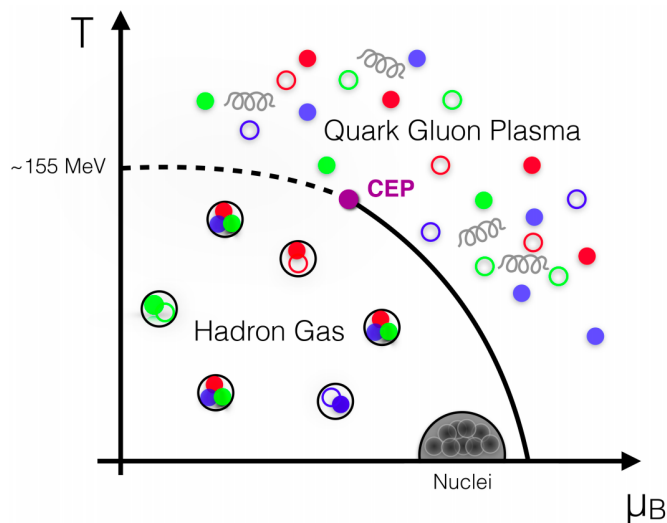


Figure 1: Conjecture of the QCD phase diagram with the temperature (T) on the vertical axis and the chemical potential (μ_B) on the horizontal axis with a hypothetical phase transition and critical end point between the hadron gas and the QGP. Figure taken from [1].

These collisions created in the experiments are the only way to heat and compress nuclear matter at significant temperatures and create a region with very high densities. In these experiments there are only two tools that can be controlled for the study of heavy ion collisions: the species of ions to collide and the center of mass energy. There are certain data that cannot be observed directly in the experiment, so it is very important to do phenomenological studies to learn more about them. The detectors of the experiment are built around the interaction point of the collision and are capable of measuring observables such as particle yields and spectra, event-by-event fluctuations of multiplicity and transverse momentum as well as the corresponding integral distributions.

The international project "Nucleon-based Ion Collider facility" NICA [2] is aimed at

the laboratory study of the properties of nuclear matter in the region of maximum baryonic density. This type of matter only existed in the early stages of the universe and inside neutron stars, however, calculations with Lattice QCD predict that the deconfinement phase transition and restoration of chiral symmetry energy densities occur. very high can be created in nuclear collisions. Experimental data on the properties of hadron production at SPS (CERN) suggest that this transition occurs within the energy range of NICA. Furthermore, this range is large enough to cover both collisions in which the plasma phase is well developed and collisions in which matter remains purely hadronic at all times. Furthermore, in addition to determining the existence and location of the transition region, it is of fundamental interest to establish the character of the associated phase transformation, that is, whether it is still a smooth crossing or has become a first-order one, such as several models predict. In the latter case, the phase diagram of strongly interacting matter must contain a critical point, and its experimental identification forms a focal point for this field of inquiry. The figure 2 shows the QCD phase diagram with the different regions in which the experiments take place.

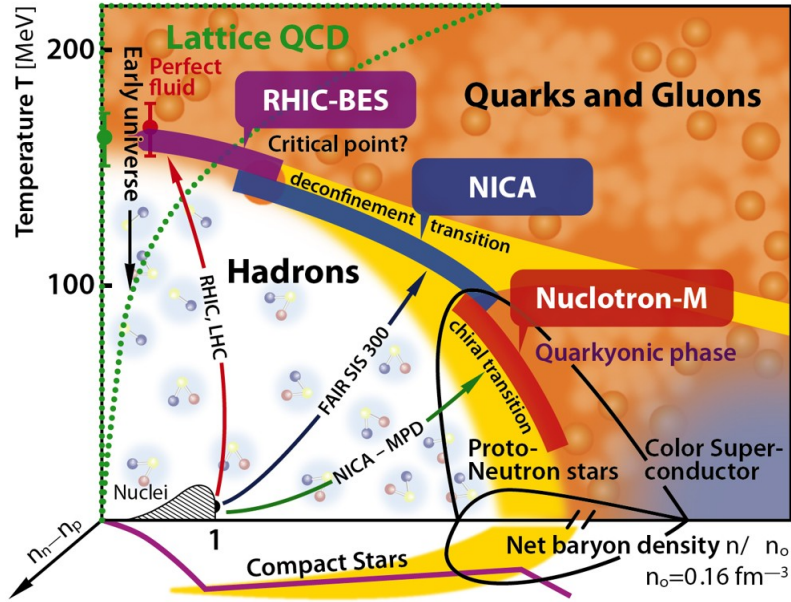


Figure 2: QCD Phase Diagram Conjecture with μ_B on the horizontal axis and Temperature T (in energy units) on the vertical axis. It also shows the regions that various experiments can access [2].

The basic configuration of NICA will allow heavy ions to be accelerated and collided, in the optimal energy range to study this phase transition. NICA will provide a variety of beam species ranging from polarized protons and deuterons to very massive gold ions. Heavy ions will be accelerated to a kinetic energy of $\sqrt{s_{NN}} = 11$ GeV and protons to $\sqrt{s_{NN}} = 27$ GeV. The heart of the NICA complex is the "Nuclotron" accelerator (which has been working at JINR since 1992) which has a maximum magnetic stiffness of 45 Tm and a circumference of 251.52 m provides the acceleration of ions at the energy of the [?]. NICA will be composed of a Booster, a superconducting synchrotron, which accumulates, cools and further accelerates heavy ions to 600 MeV/n of energy. The circumference of the amplifier is 211 meters, its magnetic structure is mounted inside the yoke of the Nuclotron. The two interaction points are prepared in the NICA collider ring: one for studies of heavy ions with the Multi-Purpose Detector (MPD), another for polarized beams for the Spin Physics Detector (SPD) experiment, and an experimental facility that will work with beams extracted in the [?] fixed-target

experiments. A schematic drawing of the NICA experiment complex with the three main experiments is shown in figure 4.

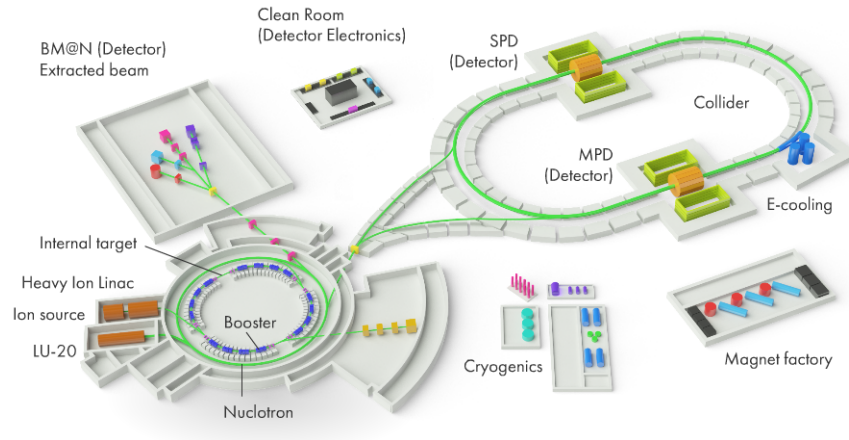


Figure 3: Schematic drawing of the NICA experiment [2]

The SPD aims to study the polarized beams of protons and deuterons to study the physics of particle spin. Measurements of asymmetries in the production of lepton pairs (Drell-Yan) in collisions of unpolarized, longitudinally and transversely polarized proton-deuteron beams using the SPD are suggested. The ultimate goal of BM@N is to carry out a research program focused on the production of foreign matter in heavy ion collisions at beam energies between 2 and 6A GeV.

The planned commissioning date of the NICA collider is at the end of 2022. At the same time, the Multi-Purpose Detector (MPD) has been designed to operate at NICA. MPD components are currently in production. The assembly of different detector subsystems on site has already started. In late 2021, the detector setup will begin cosmic data commissioning, to be ready for data collection in the first NICA rays. NICA will provide a complementary competitive research program to those of BNL, CERN and the one planned at FAIR.

The events classification by centrality of the heavy ion collisions is a key topic of the ex-

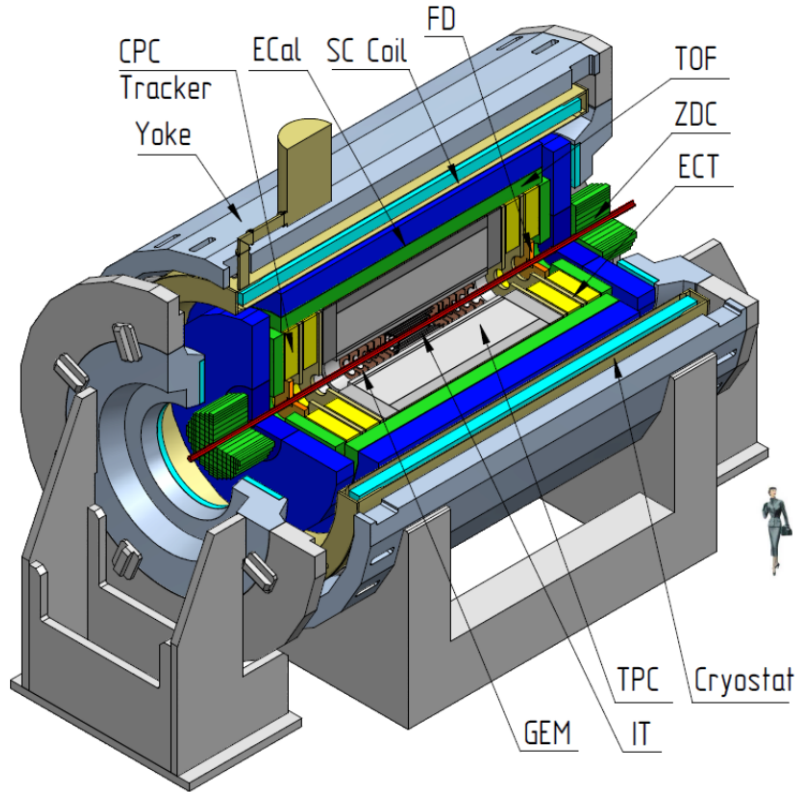


Figure 4: Schematic drawing of the Multi Purpose Detector of the NICA experiment.

periments studying a strongly excited (hot and/or dense) hadronic matter properties. It is crucial to select central collisions to study the most excited nuclear matter. Observables analysis in different centrality intervals allows to study space–time picture of the nuclear–nuclear collisions as well as hadronic matter properties, both of which impossible without centrality data involving. One of the most important observables in the experiment are the multiplicity classes, which are related to the centrality classes by impact parameter ranges (b) of the collisions.

Since the MPD/NICA complex is under development, it is of vital importance to have a simulation framework to generate studies prior to the first collider runs. The MpdRoot framework [6] is based on FairRoot and provides a powerful tool for detector performance studies, development of algorithms for reconstruction and physics analysis of the data. Ex-

tended set of event generators for heavy ion collisions are used (UrQMD, LAQGSM, HSD).

In particular, the Ultrarelativistic Quantum Molecular Dynamics (UrQMD) model [7] is a microscopic model used to simulate and study (ultra)relativistic heavy ion collisions of pp, pA and A+A in the energy range from Bevalac and SIS ($\sqrt{S_{NN}} \sim 5$ GeV) up to AGS, SPS and RHIC ($\sqrt{S_{NN}} \sim 200$ GeV). It represents a Monte Carlo solution of a large set of coupled partial integro-differential equations for the time evolution of the various phase space densities of particle species with a microscopic transport theory based on the covariant propagation of all hadrons in classical trajectories.

Project goals

- Correct the p_T cut to the multiplicity classes and compare with the results obtained without the correction in the centrality determination.
- Identify the particles using the z-variable method.
- Fit the Bethe Bloch formula with 5 parameters in the scatter plot $\langle dE/dx \rangle$ vs p_T .

Scope of work

We aim to contribute to the studies of bulk properties of this system for incoming run of MPD/NICA. For preliminary results to the first runs on the NICA complex with Bi+Bi heavy ion collisions at low energies, previous studies of first physics are necessary.

Method

For the analysis we used the Monte-Carlo official data from the MPD collaboration which are located at the NICA LHEP computing cluster [8]. Using the available data of UrQMD at the center-of-mass energy of $\sqrt{S_{NN}} = 7.7, 9, 9.2$ GeV for Bi+Bi collisions and statistics of 10^6 events for each energy which are described in [9], [10] and [11] respectively.

1 TPC acceptance

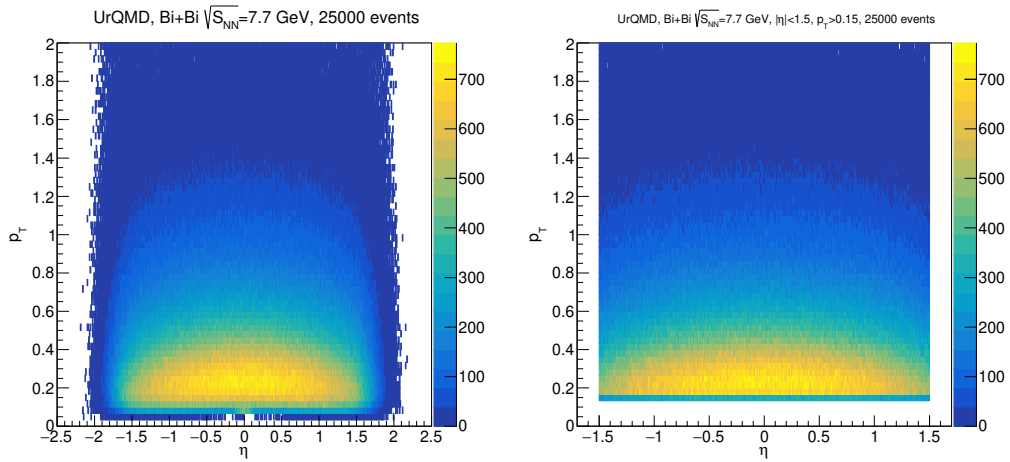


Figure 5: TPC acceptance for Bi+Bi at 7.7 GeV without cuts (left) and with cuts (right). With a difference of the number of entries in total $\Delta entries = 613935$ and per event $\Delta entries/event = 24$.

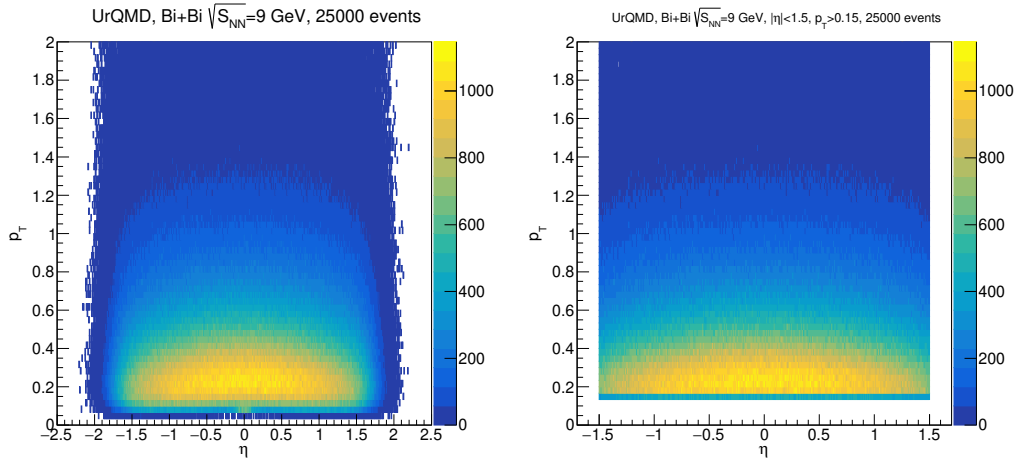


Figure 6: TPC acceptance for Bi+Bi at 9 GeV without cuts (left) and with cuts (right). With a difference of the number of entries in total $\Delta entries = 910017$ and per event $\Delta entries/event = 36$.

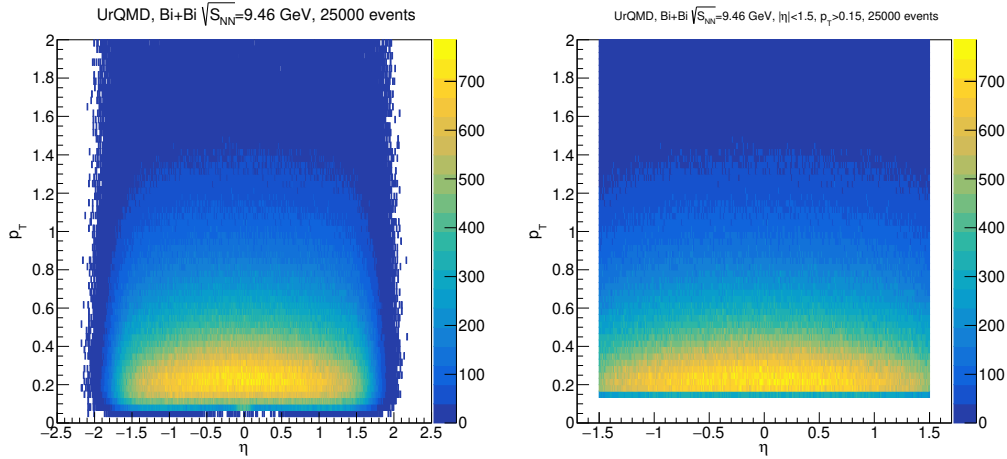


Figure 7: TPC acceptance for Bi+Bi at 9.46 GeV without cuts (left) and with cuts (right). With a difference of the number of entries in total $\Delta entries = 655222$ and per event $\Delta entries/event = 26$.

- $p_T > 0.15$ GeV/c
- $|\eta| < 0.5$ and $|\eta| < 1.3$
- Only charged particles
- $N_{hits} > 16$
- Corrected DCA values with selection of primary particles [?].
- $\sim 600,000$ events.
- Bi+Bi collisions at 7.7, 9 and 9.46 GeV [9], [10] and [11] using UrQMD.

2 Cross section vs CM Energy

To use the MC-Glauber at NICA energies we have to obtain the relation between the inelastic cross section σ_{NN}^{inel} and the center-of-mass energy $\sqrt{s_{NN}}$.

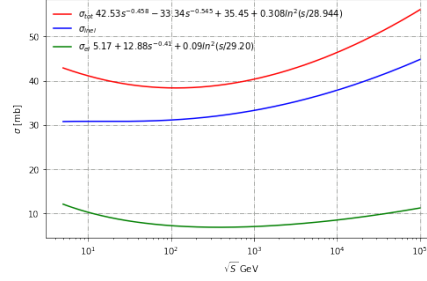


Figure 8: Overview of elastic (σ_{el}), inelastic (σ_{inel}), total (σ_{tot}) cross section for pp collisions as a function of \sqrt{S} . The red line (for pp) represent the best fit of the total cross section data by the COMPETE collaboration. The blue line refer to the inelastic cross section and is obtained as the difference between the total and inelastic fit.

3 Transverse momentum in the DST and miniDST files

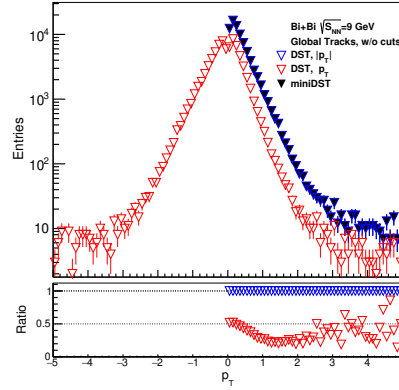


Figure 9: Transverse momentum distribution comparison between the DST and miniDST files for the Global Tracks of Bi+Bi at $\sqrt{s_{NN}} = 9$ GeV without cuts. The transverse momentum in the DST's is multiplied by the charge ($q \times p_T$) to save memory in the reconstructed files.

4 Multiplicity distributions

We obtain the multiplicity distributions with the p_T correction from the data generated in the NICA cluster:

1. UrQMD, min. bias, BiBi @ 9 GeV

<https://mpdforum.jinr.ru/t/request4-pwg3-urqmd-min-bias-bibi-9-gev/232>

2. DCM-SMM, min bias BiBi@9.2 GeV, 1 mln

<https://mpdforum.jinr.ru/t/request-16-pwg1-dcm-smm-min-bias-bibi-9-2-gev-1-mln/376>

3. Dielectrons, 15M UrQMD BiBi@9.2

<https://mpdforum.jinr.ru/t/request13-pwg4-dielectrons-15m-urqmd-bibi-9-2/375>

4. UrQMD, flow, 10M min. bias AuAu,BiBi @ 7.7 GeV

<https://mpdforum.jinr.ru/t/request-9-pwg3-urqmd-flow-10m-min-bias-auau-bibi-7-7-gev/297>

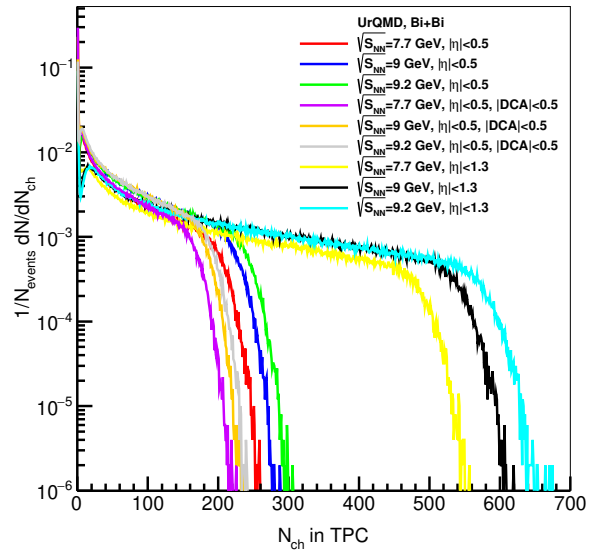


Figure 10: Multiplicity distributions.

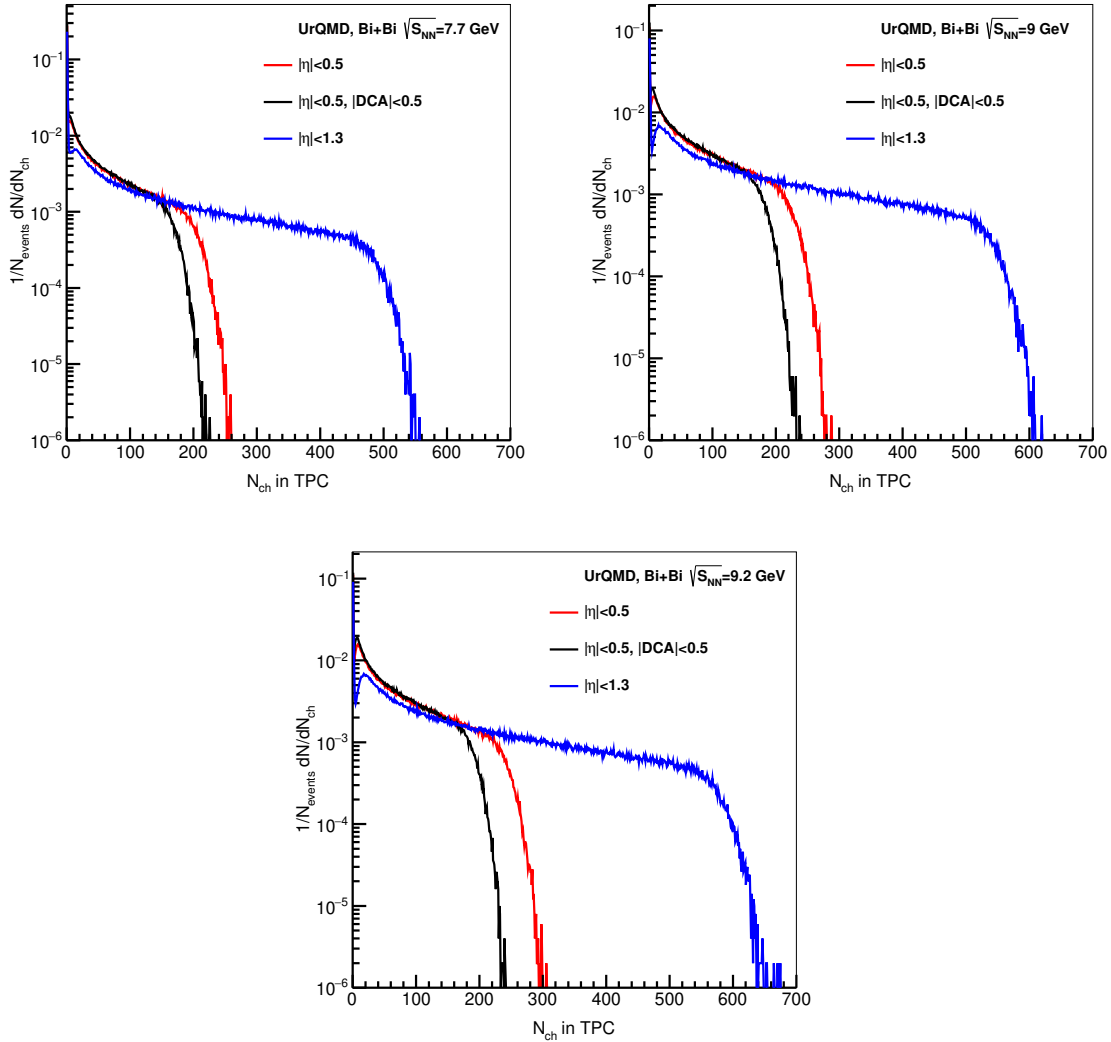


Figure 11: Multiplicity distributions of Bi+Bi collisions at 7.7, 9 and 9.2 GeV.

Centrality determination

The procedure to study the centrality classes as a function of the number of charged particles is based on the Glauber Monte Carlo model, in which two nuclei can be treated as a set of nucleons and thus their collision process can be simulated event by event quasi-independently. In the MC-Glauber approach the multiplicity of the collisions is modeled as a sum of particles produced from a set of N_a independent emitting sources ("ancestors") that depends

on the soft interactions part with an average multiplicity proportional to the number of participants N_{part} , and the hard interactions where final multiplicity is proportional to the number of binary collisions N_{coll} . The parameter f describes the relation between those two subprocesses and can change from 0 to 1 [12, 13]:

$$N_a(f) = fN_{part} + (1 - f)N_{coll}. \quad (1)$$

The average multiplicity per event is calculated using the negative binomial distribution (NBD) $P_{\mu,k}$ where the parameter k controls the width and μ is the ratio of the maximum multiplicity of the real distribution and the maximum number of ancestors:

$$M_{MC-GI}(N_a, k, f) = \sum_1^{N_a} P_{\mu,k} \times N_a. \quad (2)$$

To obtain the optimal set of parameters f , k and μ that fits better the multiplicity distribution, a minimization procedure of the χ^2 was used. Finally, the mean value of the impact parameter $\langle b \rangle$ can be extracted with the best set of parameters (f , k and μ) for the centrality classes defined by the sharp cuts in the multiplicity distribution. On the right of figure ?? is shown the multiplicity distribution from the reconstructed UrQMD events (white squares) and the MC-Glauber fit distribution (black triangles) for Bi+Bi collisions at $\sqrt{S_{NN}} = 9$ GeV.

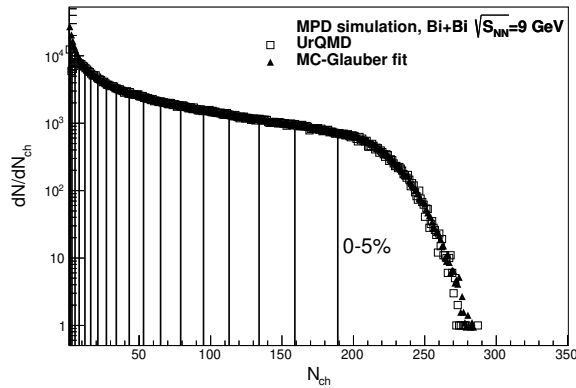


Figure 12: Multiplicity distribution for Bi+Bi at 9 GeV with the multiplicity cuts in ranges of 5%.

Results for 9 GeV

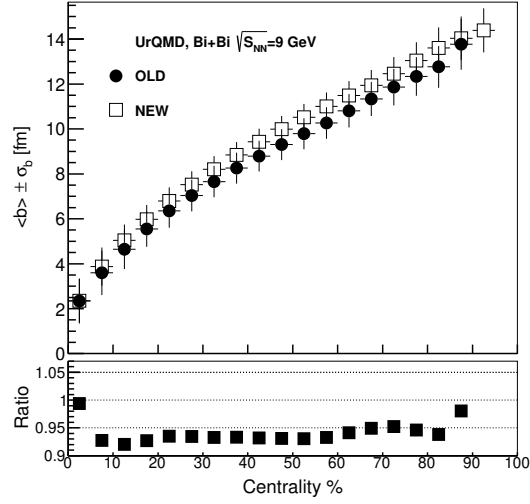


Figure 13: Comparison of the centrality with the correction in the p_T cut.

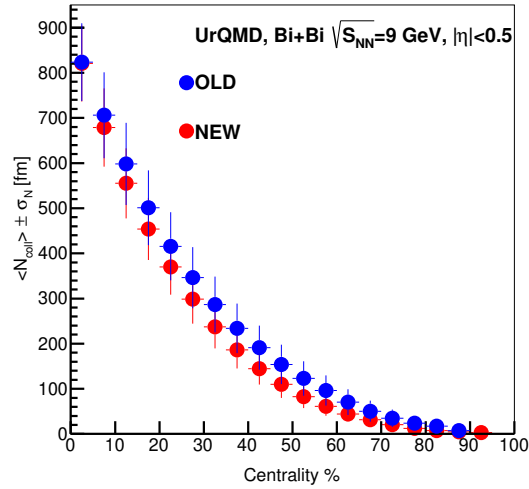


Figure 14: Comparison of the centrality with the correction in the p_T cut.

On the right plot of figure 15 the relation of $\langle b \rangle$ and centrality for the results of the MC-Glauber approach (open squares) is consistent with the results of pure UrQMD model generated data (black circles) at $\sqrt{S_{NN}} = 9$ GeV with $|\eta| < 0.5$.

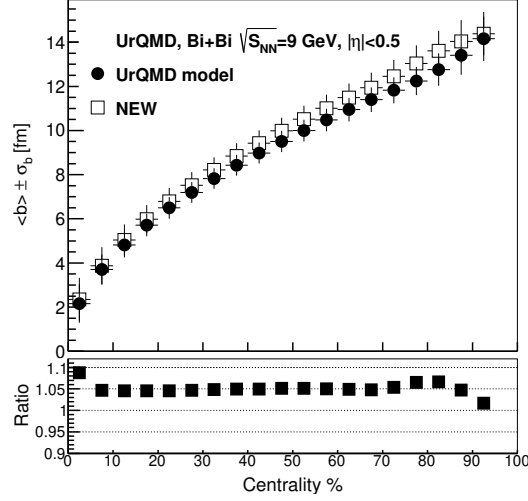


Figure 15: Comparison of the centrality with the correction in the p_T cut and the UrQMD model.

Centrality, %	N_{ch}^{min}	N_{ch}^{max}	$\langle b \rangle$, fm	RMS	b_{min} , fm	b_{max} , fm	$\langle N_{part} \rangle$	RMS	N_{part}^{min}	N_{part}^{max}	$\langle N_{coll} \rangle$	RMS	N_{coll}^{min}	N_{coll}^{max}
0 - 5	81	130	2.34	1.01	1.58	2.99	359.33	28.11	338.64	383.97	823.73	86.20	762.14	900.13
5 - 10	69	81	3.59	0.99	2.99	4.15	319.98	34.03	297.97	338.64	705.92	95.03	644.34	762.14
10 - 15	59	69	4.64	0.88	4.15	5.13	281.17	33.96	261.43	297.97	597.94	91.11	543.47	644.34
15 - 20	50	59	5.54	0.79	5.13	5.96	245.05	31.97	228.60	261.43	501.07	82.97	456.83	543.47
20 - 25	42	50	6.35	0.75	5.96	6.69	212.09	30.14	199.07	228.60	415.71	75.63	382.16	456.83
25 - 30	36	42	7.03	0.71	6.69	7.35	184.27	27.93	172.50	199.07	346.16	67.73	317.65	382.16
30 - 35	30	36	7.66	0.70	7.35	7.95	159.51	26.41	148.61	172.50	286.77	61.70	261.84	317.65
35 - 40	25	30	8.25	0.69	7.95	8.51	136.70	24.53	127.12	148.61	234.04	54.94	213.59	261.84
40 - 45	21	25	8.79	0.68	8.51	9.05	117.23	22.74	107.82	127.12	191.25	48.79	172.01	213.59
45 - 50	17	21	9.30	0.69	9.05	9.56	99.49	21.40	90.52	107.82	154.11	43.76	136.39	172.01
50 - 55	14	17	9.79	0.69	9.56	10.06	83.79	19.67	75.04	90.52	122.87	38.33	106.19	136.39
55 - 60	11	14	10.26	0.71	10.06	10.55	69.61	18.26	61.23	75.04	96.23	33.62	80.94	106.19
60 - 65	8	11	10.81	0.74	10.55	11.04	54.88	16.78	48.95	61.23	70.52	28.68	60.19	80.94
65 - 70	6	8	11.34	0.76	11.04	11.54	42.36	14.77	38.08	48.95	50.36	23.24	43.50	60.19
70 - 75	4	6	11.87	0.82	11.54	12.06	31.69	13.21	28.48	38.08	34.78	19.01	30.30	43.50
75 - 80	3	4	12.34	0.86	12.06	12.63	23.69	11.28	20.02	28.48	24.08	14.84	19.92	30.30
80 - 85	2	3	12.76	0.93	12.63	13.28	17.92	9.95	12.56	20.02	17.10	12.16	11.47	19.92
85 - 90	1	2	13.77	1.13	13.28	14.05	8.75	7.32	5.96	12.56	7.36	7.83	3.83	11.47

Results for 9 GeV before correction.

$$f = 0.83 \pm 0.046 \mu = 0.458479 \pm 0.217888 k = 1 \pm 0.253 \chi^2 = 1.20338 \pm 0.106073$$

Centrality, %	N_{ch}^{min}	N_{ch}^{max}	$\langle b \rangle$, fm	RMS	b_{min} , fm	b_{max} , fm	$\langle N_{part} \rangle$	RMS	N_{part}^{min}	N_{part}^{max}	$\langle N_{coll} \rangle$	RMS	N_{coll}^{min}	N_{coll}^{max}
0 - 5	189	291	2.35	0.97	1.63	3.15	359.46	26.60	334.05	386.07	820.71	84.20	746.39	899.68
5 - 10	159	189	3.87	0.84	3.15	4.43	310.60	30.03	287.69	334.05	678.69	86.82	615.51	746.39
10 - 15	134	159	5.04	0.71	4.43	5.50	265.62	27.81	246.57	287.69	555.18	77.56	504.30	615.51
15 - 20	113	134	5.98	0.64	5.50	6.41	227.22	25.53	210.25	246.57	454.11	68.94	410.26	504.30
20 - 25	95	113	6.79	0.61	6.41	7.21	193.96	23.50	178.30	210.25	369.89	61.15	331.15	410.26
25 - 30	79	95	7.52	0.59	7.21	7.91	164.55	21.76	150.30	178.30	298.37	54.27	264.95	331.15
30 - 35	65	79	8.21	0.58	7.91	8.54	138.12	19.96	125.83	150.30	237.12	47.53	209.88	264.95
35 - 40	53	65	8.84	0.58	8.54	9.13	114.91	18.26	104.51	125.83	186.15	41.27	164.34	209.88
40 - 45	43	53	9.43	0.58	9.13	9.68	94.86	16.55	85.96	104.51	144.47	35.21	126.95	164.34
45 - 50	34	43	9.99	0.59	9.68	10.22	77.20	15.04	69.85	85.96	110.06	30.02	96.49	126.95
50 - 55	27	34	10.52	0.60	10.22	10.74	62.03	13.52	55.88	69.85	82.48	25.15	71.89	96.49
55 - 60	21	27	11.01	0.62	10.74	11.25	49.46	12.11	43.81	55.88	61.24	20.82	52.26	71.89
60 - 65	16	21	11.48	0.64	11.25	11.76	38.53	10.74	33.45	43.81	44.23	16.91	36.83	52.26
65 - 70	12	16	11.94	0.67	11.76	12.26	29.48	9.42	24.64	33.45	31.33	13.53	24.95	36.83
70 - 75	8	12	12.46	0.74	12.26	12.76	21.17	8.14	17.33	24.64	20.64	10.48	16.08	24.95
75 - 80	5	8	13.04	0.82	12.76	13.26	13.93	6.47	11.52	17.33	12.33	7.35	9.78	16.08
80 - 85	3	5	13.60	0.91	13.26	13.74	8.86	4.82	7.29	11.52	7.16	4.88	5.68	9.78
85 - 90	2	3	14.04	0.96	13.74	14.22	6.03	3.52	4.80	7.29	4.54	3.31	3.48	5.68
90 - 95	1	2	14.39	0.98	14.22	14.70	4.25	2.50	4.32	4.80	3.00	2.24	2.95	3.48

Results for 9 GeV after correction.

5 Particle Identification

Bethe was the first to calculate, in 1930, the average energy loss with a quantum theory of collision between the travelling particle and a single atom. After adding the energy lost to all the atoms in the vicinity of the particle, the energy loss per unit of pathlength is given by:

$$\left\langle \frac{dE}{dx} \right\rangle = \frac{4\pi N e^4}{m c^2 \beta^2} z^2 \left(\ln \frac{2 m c^2 \beta^2 \gamma^2}{I} - \beta^2 \right) \quad (3)$$

In this equation $m c^2$ is the rest energy of the electron, z the charge of the travelling particle, N the number density of electrons in the matter traversed, e the elementary charge, β the velocity of the travelling particle in terms of the velocity c of light, and $\gamma^2 = 1/(1 - \beta^2)$, so $\beta\gamma = p/m$ in natural units. The symbol I denotes the mean excitation energy of the atom.

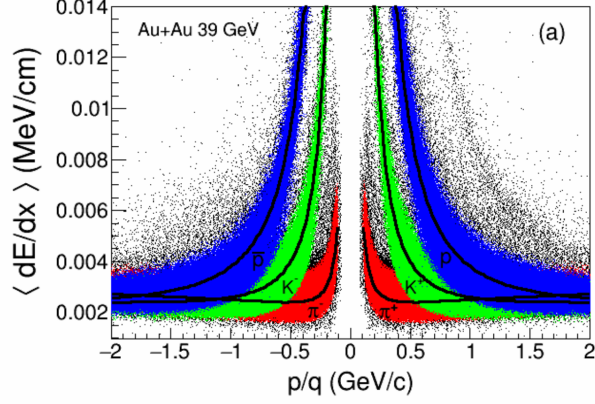


Figure 16: The dE/dx of charged tracks at midrapidity ($|y| < 0.1$) plotted as function of rigidity (p/q) in Au+Au collisions at $\sqrt{S_{NN}} = 39$ GeV. The various bands correspond to different particles such as π^\pm , K^\pm , p and \bar{p} . The curves represent the Bichsel expectation values of the corresponding particles.

The $\langle dE/dx \rangle$ distribution for a fixed particle type is not Gaussian. It has been shown that a better Gaussian variable, for a given particle type, is the z -variable, defined as [14]:

$$z_X = \ln \left(\frac{\langle dE/dx \rangle}{\langle dE/dx \rangle_X} \right) \quad (4)$$

Where x is the particle type (e^\pm , π^\pm , K^\pm , p , or \bar{p}) and $\langle dE/dx \rangle_X$ is the corresponding mean value of the $\langle dE/dx \rangle$ distribution for the X particle.

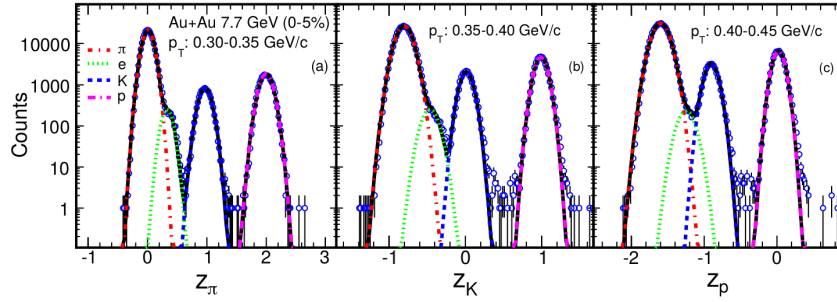


Figure 17: The z_π , z_K , and z_p distributions for positively charged hadrons (π , K , and p) at midrapidity ($|\eta| < 0.1$) in the TPC for various p_T ranges in Au+Au collisions at $\sqrt{S_{NN}} = 7.7$ GeV. The curves are Gaussian fits representing contributions from pions (dash-dotted, red), electrons (dotted, green), kaons (dashed, blue), and protons (long dash-dotted, magenta). Uncertainties are statistical only.

5.1 Results for 9 GeV

Obtain the $\langle dE/dx \rangle$ vs rigidity (p_T/q).

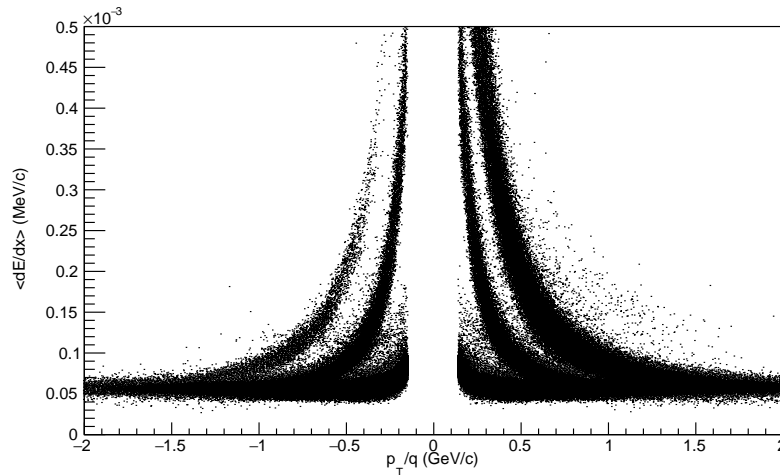


Figure 18: The $\langle dE/dx \rangle$ of charged tracks at midrapidity ($|\eta| < 0.5$) plotted as function of rigidity (p_T/q) in Bi+Bi collisions at $\sqrt{S_{NN}} = 9$ GeV.

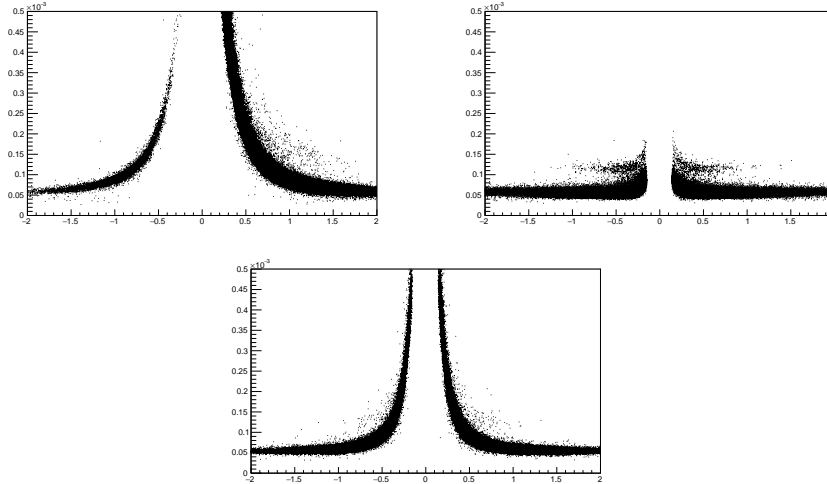


Figure 19: The $\langle dE/dx \rangle$ of charged tracks at midrapidity ($|\eta| < 0.5$) plotted as function of rigidity (p/q) in Bi+Bi collisions at $\sqrt{S_{NN}} = 9$ GeV in a range of $0.3 < p_T < 0.35$ selecting protons, pions and Kaons with the MC-Tracks.

Cut in a p_T range.

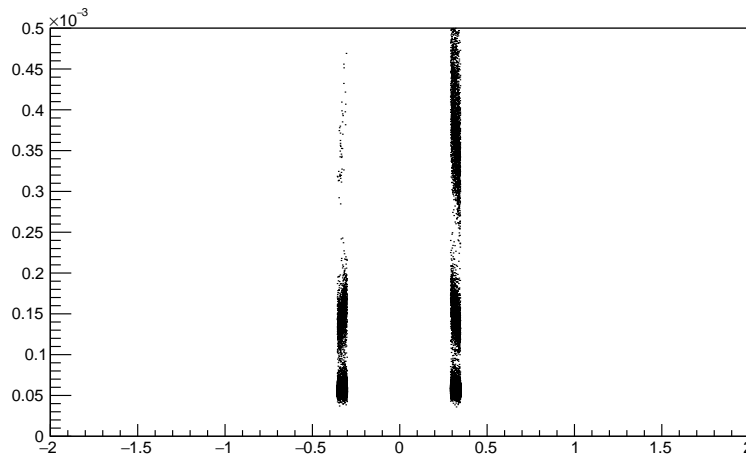


Figure 20: The $\langle dE/dx \rangle$ of charged tracks at midrapidity ($|\eta| < 0.5$) plotted as function of rigidity (p/q) in Bi+Bi collisions at $\sqrt{S_{NN}} = 9$ GeV in a range of $0.3 < p_T < 0.35$.

Obtain the $\langle dE/dx \rangle$ distribution.

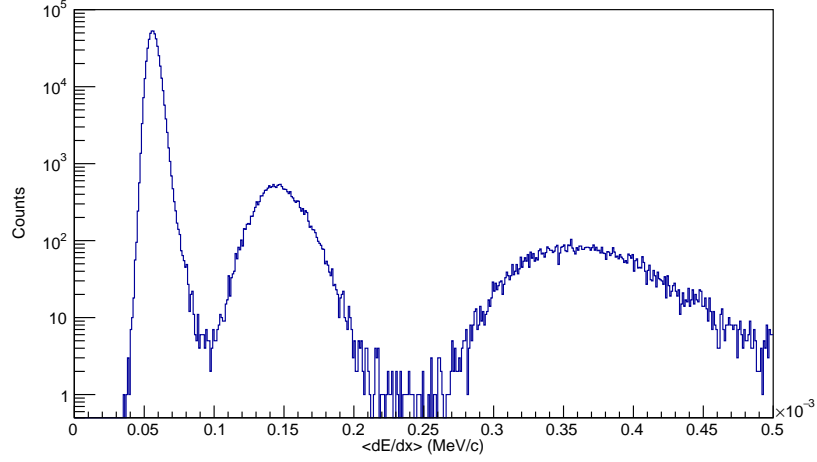


Figure 21: The $\langle dE/dx \rangle$ distribution of charged tracks at midrapidity ($|\eta| < 0.5$) for Bi+Bi collisions at $\sqrt{S_{NN}} = 9$ GeV in a range of $0.3 < p_T < 0.35$ selecting all particles.

Select the $\langle dE/dx \rangle$ distribution for each particle and extract the mean value ($\langle dE/dx \rangle_X$).

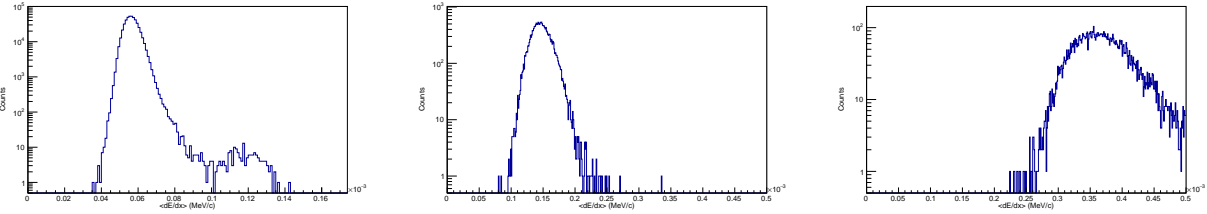


Figure 22: The $\langle dE/dx \rangle$ distribution of charged tracks at midrapidity ($|\eta| < 0.5$) for Bi+Bi collisions at $\sqrt{S_{NN}} = 9$ GeV in a range of $0.3 < p_T < 0.35$ selecting Pions (left) and Kaons (middle) and Protons (right) with the MC-Tracks.

Fit the Z-variable distribution selecting with the MC-Tracks.

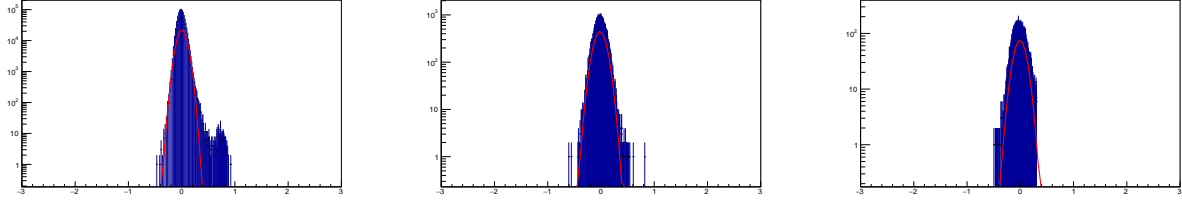


Figure 23: The z – *variable* distribution of charged tracks at midrapidity ($|\eta| < 0.5$) for Bi+Bi collisions at $\sqrt{S_{NN}} = 9$ GeV in a range of $0.3 < p_T < 0.35$ selecting Pions (left) and Kaons (middle) and Protons (right) with the MC-Tracks.

Fit the Z-variable without MC-Track selection.

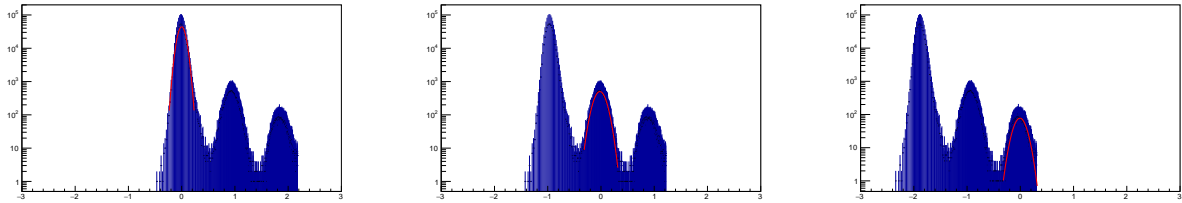


Figure 24: The z – *variable* distribution of charged tracks at midrapidity ($|\eta| < 0.5$) for Bi+Bi collisions at $\sqrt{S_{NN}} = 9$ GeV in a range of $0.3 < p_T < 0.35$ for z_π (left) and z_K (middle) and z_P (right).

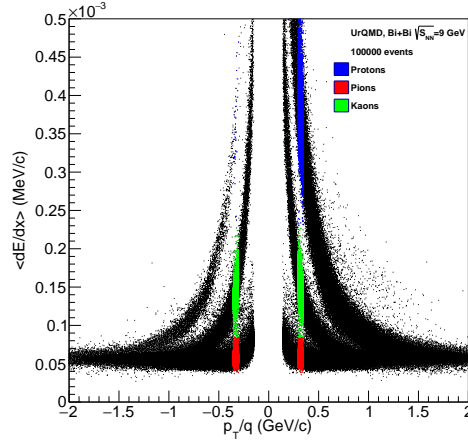


Figure 25: The $\langle dE/dx \rangle$ distribution of charged tracks at midrapidity ($|\eta| < 0.5$) for Bi+Bi collisions at $\sqrt{S_{NN}} = 9$ GeV in a range of $0.3 < p_T < 0.35$ selecting the Protons, Pions and Kaons with the z -variable criteria.

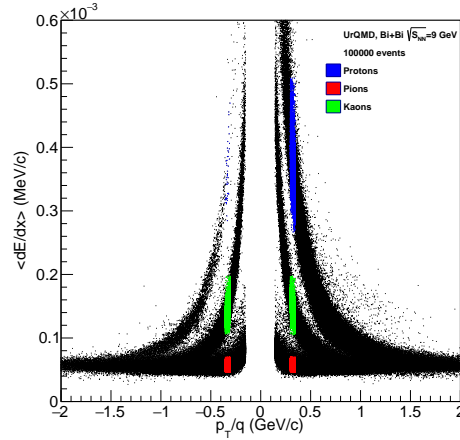


Figure 26: The $\langle dE/dx \rangle$ distribution of charged tracks at midrapidity ($|\eta| < 0.5$) for Bi+Bi collisions at $\sqrt{S_{NN}} = 9$ GeV in a range of $0.3 < p_T < 0.35$ selecting the Protons, Pions and Kaons with the z -variable criteria choosing $3 - \sigma$ for each particle fit.

In the model of Allison and Cobb for each transferred energy:

$$\left\langle \frac{dE}{dx} \right\rangle = \frac{p_1}{\beta^{p_4}} \left\{ p_2 + \beta^{p_4} - \ln \left[p_3 + \left(\frac{1}{\beta\gamma} \right)^{p_5} \right] \right\} \quad (5)$$

Where the p_i are five free parameters for the fit and $\beta^2 = p^2/(m^2 + p^2)$.

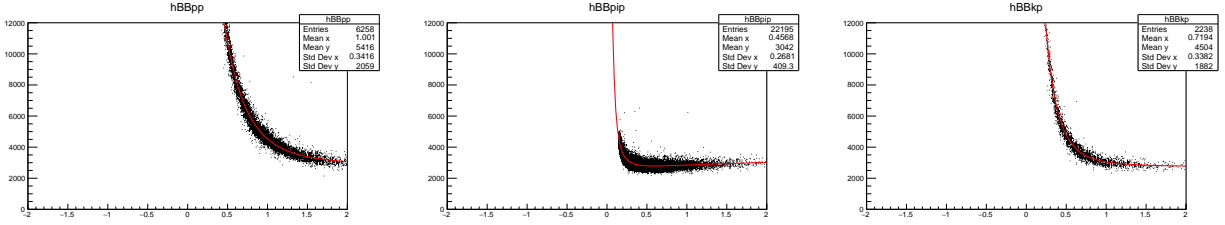


Figure 27: Bethe Bloch fit for positive protons (left), pions (middle) and kaons (right).

	p^+	π^+	K^+
p_1	-6818.6 ± 190.758	-100.307 ± 2.96732	-951.231 ± 55.426
p_2	1.63195 ± 0.0604219	-20.835 ± 0.68985	-2.53809 ± 0.210215
p_3	2.84047 ± 0.138809	1.28538 ± 0.275867	0.509255 ± 0.0321495
p_4	0.0423965 ± 0.049016	2.23885 ± 0.0283511	0.955075 ± 0.0488958
p_5	2.86607 ± 0.0602418	-3.0304 ± 0.0894649	3.8073 ± 0.155543

Table 1: The corresponding 5 parameters for each positive particle.

Conclusions

- We calculated centrality classes for Bi+Bi collisions at center-of-mass energies of $\sqrt{S_{NN}} = 9$ GeV with the corresponding p_T correction.
- The particle identification using the z-variable method was implemented for the miniDST files.
- We used the Bethe Bloch fit for 5 parameters for the positive particles in the scatter plot $\langle dE/dx \rangle$ vs p_T .

Acknowledgments

I would like to thank my supervisor Dr. Alexey Aparin for giving me the opportunity to participate in his project in the Student Program 2022 at JINR and for instructing me during the last year since the Interest Program Wave 3. I would also like to thank the Organizing Committee of the Student Program 2022 at JINR for the great opportunity to participate in a project that will help me in my professional future and for giving me the support to live one of the most rewarding experiences of my life.

Science bring nations together.

Bibliography

- [1] Maria Elena Tejeda-Yeomans. Heavy-ion physics: freedom to do hot, dense, exciting QCD. In 10th CERN–Latin-American School of High-Energy Physics, 4 2020.
- [2] Nuclotron-based Ion Collider fAcility (NICA) <http://nica.jinr.ru/physics.php>
- [3] NKekelidze, V.D., Matveev, V.A., Meshkov, I.N. et al. Project Nuclotron-based Ion Collider fAcility at JINR. Phys. Part. Nuclei 48, 727–741 (2017). URL: <https://doi.org/10.1134/S1063779617050239>
- [4] MPD official website: <http://mpd.jinr.ru/experiment/>
- [5] L Yordanova and V Vasendina. “MPD Detector at NICA”. In: Journal of Physics: Conference Series 503 (Apr. 2014), p. 012041. DOI: [10.1088/1742-6596/503/1/012041](https://doi.org/10.1088/1742-6596/503/1/012041)
- [6] MpdRoot official site: <http://mpd.jinr.ru/>
- [7] UrQMD official site: <https://urqmd.org/>
- [8] NICA Cluster: <http://mpd.jinr.ru/howto-work-with-nica-cluster/>
- [9] Monte-Carlo request for @7.7 GeV events of the MPD collaboration for PWG4: <https://mpdforum.jinr.ru/t/request-9-pwg3-urqmd-flow-10m-min-bias-auau-bibi-7-7-gev/297>
- [10] Monte-Carlo request for @9 GeV events of the MPD collaboration for PWG: <https://mpdforum.jinr.ru/t/request4-pwg3-urqmd-min-bias-bibi-9-gev/232>
- [11] Monte-Carlo request for @9.46 GeV events of the MPD collaboration for PWG3: <https://mpdforum.jinr.ru/t/request5-pwg4-dielectrons-10m-minbias-bibi-9-46/235>
- [12] Parfenov, Petr and Idrisov, Dim and Luong, Vinh Ba and Taranenko and Arkadiy. Relating Charged Particle Multiplicity to Impact Parameter in Heavy-Ion Collisions at NICA Energies. DOI: [10.3390/particles4020024](https://doi.org/10.3390/particles4020024)
- [13] P. Parfenov, I. Segal and D. Idrisov and V.B. Luong and A. Taranenko and A. Demanov and A. Truttse and E. Volodikhin. Centrality Determination in Heavy-ion Collisions with MPD Detector at NICA. DOI: [10.5506/APhysPolBSupp.14.503](https://doi.org/10.5506/APhysPolBSupp.14.503)
- [14] STAR Collaboration. Bulk properties of the medium produced in relativistic heavy-ion collisions from the beam energy scan program. DOI: [10.1103/PhysRevC.96.044904](https://doi.org/10.1103/PhysRevC.96.044904)
- [15] Centrality determination:
<https://github.com/FlowNICA/CentralityFramework>